

A New Paradigm for Turbulent Transport Across a Steep Gradient in Toroidal Plasmas

H. S. Xie,^{1,*} Y. Xiao,^{1,†} and Z. Lin^{2,3}

¹*Institute for Fusion Theory and Simulation, Department of Physics,
Zhejiang University, Hangzhou, 310027, People's Republic of China*

²*Department of Physics and Astronomy, University of California, Irvine, California 92697, USA*

³*Fusion Simulation Center, School of Physics, Peking University, Beijing 100871, China*

(Dated: February 2, 2017)

First principle gyrokinetic simulation of the edge turbulent transport in toroidal plasmas finds a reverse trend in the turbulent transport coefficients under strong gradients. It is found that there exist both linear and nonlinear critical gradients for the nonmonotonicity of transport characteristics. The discontinuity of transport flux slope around the turning gradient shows features of second order phase transition. Under strong gradient the most unstable modes are in non-ground eigenstates with unconventional mode structures, which significantly reduces the effective correlation length and thus reverse the transport trend. Our results suggest a completely new mechanism for the low to high confinement mode transition without invoking shear flow or zonal flow. [accepted by Phys. Rev. Lett.]

With input power increasing, a sudden transport ‘phase’ with formation of edge transport barrier is found experimentally in fusion plasmas [1], which is called the high (H) confinement mode to distinguish from the conventional low (L) confinement mode, where no steep gradients exist in the plasma profiles. Transport barriers, also recognized in other systems, such as in geophysical and atmospheric sciences [2], can be universal and important. The H-mode plasmas store twice more energy than that in the L-mode, thus enabling high fusion gain. The H-mode is the baseline operation scenario of the International Thermonuclear Experimental Reactor (ITER) [3]. The L-H transition involves a discontinuous change of the transport characters and the underlying mechanism remains elusive [4]. The transition between the multiple equilibrium states resembles the continuous (or second order) phase transition of Landau [5], a critical phenomenon widely existing in nature. An improved understanding of the transition physics is not only important for fusion plasmas, but leads to a new paradigm for the nonlinear physics in the laboratory and universe.

Several theories have been proposed for the transport characteristic change [6–9] or the sudden L-H transition [10, 11], where generally shear or zonal flow is invoked. But none of these theories have been fully verified by first principle simulation or validated by fusion experiment. In addition, due to many inherent *ad hoc* assumptions on the kinetic physics, these theories may only be qualitatively correct. Recently, several fluid models (cf. [12]) have also produced some of the essential features of the L-H transition, i.e., two transport ‘phases’ are found by increasing input power. These fluid simulation results may not be conclusive due to overlook of essential kinetic physics. A fully kinetic simulation of the L-H transition is still precluded due to the multiple temporal and spatial scale nature of the problem. The gyrokinetic simulation is so far still one of the best tools to study

the kinetic physics in the edge, although the validity of gyrokinetics under strong gradients is still under active research. When studying low frequency drift wave turbulence in the tokamak edge, the gyrokinetics [13] may still be valid for $R/L_T \sim 100$, where $\rho_i/L_T \sim 0.1$, satisfying the gyrokinetic assumption $\rho_i/L_T \ll 1$. In this work, we only consider electrostatic drift wave turbulence by varying density/temperature gradients while fixing the density/temperature in the simulation. Our gyrokinetic simulation [13, 14] using the GTC code [15, 16] shows that both the linear and nonlinear physical characteristics change nonmonotonically with a turning point at some critical gradient, which divides the gradient space into a weak gradient region (L-mode) and a strong gradient region (H-mode). It is known that drift wave turbulence can lead to anomalous transport [17]. It is also commonly accepted that stronger gradient leads to higher transport coefficients [18, 19]. Based on large scale global gyrokinetic simulations using the GTC code, we report here for the first time that the turbulent transport coefficients in toroidal plasmas can be reversed under strong gradient, i.e., larger gradient leads to smaller transport coefficient. The slope of the transport flux also shows a discontinuous change around the turning gradient, similar to the second order phase transition of Landau [5]. The underlying physics is found to be closely related to the unconventional mode structure under strong gradients, which significantly reduces the radial correlation length. These novel findings may suggest a completely new mechanism for the L-H transition without invoking shear flow or zonal flow.

The GTC code is a well-benchmarked global gyrokinetic particle simulation code [15, 20–22], suitable for simulating both electrostatic and electromagnetic drift wave turbulence [17]. In the low beta limit, we only use the electrostatic capability of the GTC code. The simulation parameters are taken from typical H-mode exper-

iments of the HL-2A tokamak [23, 24] using deuterium as the ion species, with on-axis toroidal magnetic field $B_0 = 1.35T$, minor radius $a = 40cm$, major radius $R_0 = 165cm$, safety factor $q = 2.7$, magnetic shear $s = 0.5$, plasma temperature $T_e = T_i = 200eV$, plasma density $n_e(r) = n_i = 4.0 \times 10^{12}cm^{-3}$. Assuming that the time scale for electron-ion energy exchange is shorter than the profile relaxation time scale, we set in the simulation the plasma profile gradients $R_0/L_{T_i} = R_0/L_{T_e} = R_0/L_n$, where L_{T_i} , L_{T_e} and L_n are the scale lengths for ion temperature, electron temperature and particle density, respectively, i.e., $L_T^{-1} \equiv -d\ln T/dr$. Therefore, we keep $\eta = L_n/L_T = 1$ throughout this article. We note that one of the most important parameters is the peaking gradient [23]. In addition, circular cross-section is assumed for equilibrium magnetic flux surface.

Using the preceding experimental parameters, we carry out a series of turbulence simulations by scanning the plasma profile gradients. In the simulations, we use number of grids $150 \times 1200 \times 32$ in the radial, poloidal and parallel direction respectively which leads to a grid size $\sim 0.5\rho_i$, and 50 ions/electrons per cell to reduce the numeric noise. A larger number of grids and more particles per cell are used and a satisfactory convergence can be obtained for the simulation results. Zero boundary conditions are used at $r = 0.7a$, and $1.0a$. The time history of the volume averaged turbulent heat conductivity and particle diffusivity are shown in Fig. 1(a)-(c) for three strong gradients, $R_0/L_T = 30, 50, 100$, where the heat conductivity χ_j is defined from the heat flux $q_j = \int dv^3 (\frac{1}{2}m_j v^2 - \frac{3}{2}T_j) \delta v_E \delta f_j \equiv n_j \chi_j \nabla T_j$, $j = i, e$, and the particle diffusivity D_j is defined from the particle flux $D_j = \int dv^3 \delta v_E \delta f_j$, with v_E is the $E \times B$ drift caused by turbulence. As shown in Fig. 1, both heat conductivity and particle diffusivity decrease with the temperature gradient in the strong gradient region. This is contradictory to the common knowledge that stronger gradient leads higher transport coefficient [18]. This phenomenon is further illustrated in Fig. 2(a) by comparing the electron diffusivity for different gradients, where the diffusivity is obtained by the time average of the saturated value in the nonlinear stage before the quasilinear flattening of plasma profile occurs. The electron diffusivity first increases with the gradient, which is consistent with previous studies [18]. However, when we continue to increase the gradient after some critical value, as shown in Fig. 1, stronger gradient leads to lower particle diffusivity. The pink dash line is following the conventional trend by artificial extrapolation [18]. This reverse trend of the transport coefficients also holds for ion and electron heat transport, which can be seen in Fig. 1 (a) or (b). We note that this is the first time that such extraordinary behavior is observed for the turbulent transport under strong gradient. In Fig. 2(b) for the electron flux vs. R_0/L_T , a turning point for the gradient drive appears, and the particle flux reaches a saturation level, or

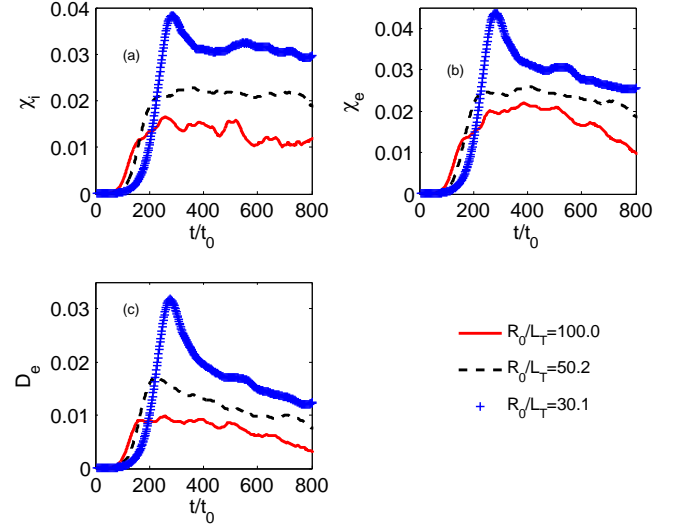


FIG. 1: Time history for three volume averaged physical quantities: (a) ion heat conductivity; (b) electron heat conductivity; (c) electron particle diffusivity under three strong temperature gradients, where $t_0 = 0.002c_s/R_0$ is time step size.

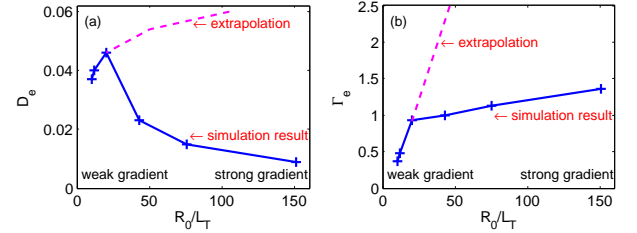


FIG. 2: Time averaged electron particle diffusivity (a) and electron particle flux (b) for different temperature gradients. A turning point (critical gradient) is found for the trend of the transport coefficients.

increases much slower, when the gradient is beyond the turning point, clearly showing a discontinuous change of the slope of the particle flux. This provides strong evidence for the formation of gradient transport barrier, even though no bifurcation occurs. If one adds more power to the core plasma than the pedestal can exhaust, the L-H transition can occur due to the gradient transport barrier, which could explain the mystery of the L-H transition, namely the input power should exceed a certain level in order to trigger the L-H transition.

Next we examine the zonal flow effect on the nonlinear physics under strong gradient. A previous study using the GTC code has shown that for the TEM mode the zonal flow can reduce the turbulent transport significantly ($> 50\%$) under weak gradient ($R_0/L_T = 6.9$) [21]. However, under strong gradient, Fig. 3 shows that the zonal flow has little effect in regulating turbulence. The weak importance of zonal flow near the edge is also reported in a recent H-mode experiment by Ref. [25].

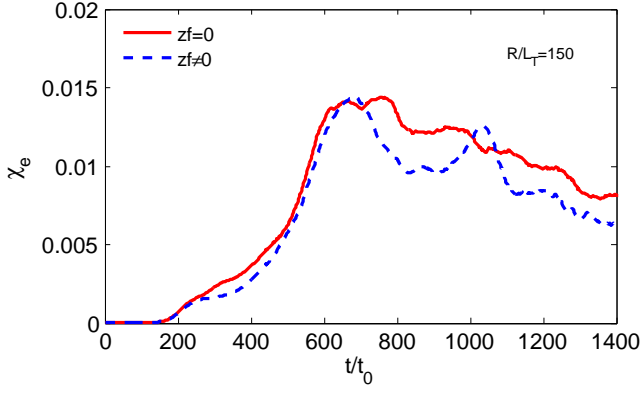


FIG. 3: Time history of electron heat conductivity in the nonlinear gyrokinetic simulation are shown for two cases under strong gradient: with and without zonal flow. The green dashed line represents simulation with zonal flow self-consistently generated. For the red solid line, the zonal flow is artificially removed from simulation.

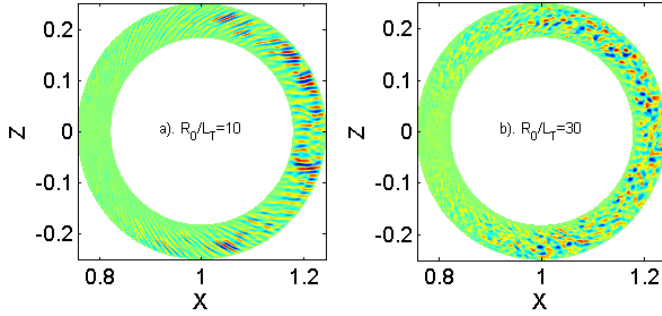


FIG. 4: 2D turbulence intensity in the poloidal plane for nonlinearly weak gradient $R_0/L_T = 10$ and nonlinearly strong gradient $R_0/L_T = 30$.

The preceding nonlinear results in Fig. 2 and Fig. 3 can be further understood by a random walk model, i.e., the transport coefficients such as the particle diffusivity D , agree with $D \sim l_c^2/\tau_c$, where l_c is the correlation length and τ_c is the correlation time. By linking $\sim l_c$ with characteristic perpendicular wavelength and τ_c with the linear growth rate, a simplest model of this type gives $D \sim (\gamma_k/k_\perp^2) \propto \gamma_k$. A rough estimate for the linear growth rate gives $\gamma_k \propto \nabla T$, thus we have $D \propto \nabla T$, which leads to the Taroni-Bohm model [26]. However, this model breaks down for large gradients, as shown in Fig. 2, as the linear growth rate γ_k (inverse of the correlation time τ_c) does not increase much with the gradient (see Fig. 6). On the other hand, the correlation length l_c should be reduced dramatically in the strong gradient region, as implied by Fig. 1. Fig. 4 shows two typical eddy size for the nonlinearly strong gradient ($R_0/L_T = 30$) and the nonlinearly weak gradient ($R_0/L_T = 10$). The zonal flow is excluded in these simulations to manifest the turbulence mode structure. We can see strong streamer structures for the case with $R_0/L_T = 10$, which shows

elongated radial eddies in Fig. 4(a) and hence large radial correlation length. The zonal flow can cut through and stretch these streamer structures and therefore can effectively reduce the transport. However, under stronger gradient $R_0/L_T = 30$, the eddy size becomes smaller and zonal flow may no longer cut through them, which can minimize the regulation effect of the zonal flow, as shown in Fig. 3.

The reverse trend of the transport coefficient in the strong gradient region can be reasonably explained by the smaller eddy size and hence smaller correlation length, which could possibly be induced by the unconventional mode structures of non-ground eigenstates of micro-instabilities [27]. To examine the physics mechanism for this reverse transport trend under strong gradient, we thus further perform a linear simulation for the most unstable mode with toroidal mode number $n = 20$, since that the discontinuous change in the nonlinear transport may be related to the discontinuity in the linear eigenmode characteristics. As shown by time history and spectrum analysis of selected unstable mode in Fig. 5 (for poloidal mode number $m = 51$), two distinct frequencies clearly coexist in electron diamagnetic direction for the linear simulation. Suppose that the 3D (three dimensional) mode structure of the electrostatic potential is represented by the Fourier series $\delta\phi(r, \theta, \zeta, t) = e^{in\zeta - i\omega t} \sum_m \delta\phi_m(r) e^{-im\theta}$, where $\omega = \omega_r + i\gamma$ is the mode frequency. We proceed to examine the mode frequency variation under different gradients. As shown in Fig. 6, there exists a clearly frequency jump from low frequency ($\omega_r < 3\omega_s$, $\omega_r < \gamma$) to high frequency ($\omega_r > 10\omega_s$, $\omega_r \gg \gamma$) branch, where the normalized frequency $\omega_s = 1/t_s \equiv c_s/R_0$ and $c_s \equiv \sqrt{T_e/m_i}$. Around the critical jump gradient ($R_0/L_T \simeq 70$), two branches of the eigenmode coexist at the initial linear stage due to similar growth rates, as shown in Fig. 5. The low frequency branch shows a conventional ballooning structure localized at the outside mid-plane (ground eigenstate), whereas the high frequency branch shows an unconventional mode structure which can localize at almost arbitrary poloidal positions or with multiple peaks (non-ground eigenstate) [23, 27]. For the weak gradient (L-mode), the most unstable mode is in the ground state. However, the most unstable mode can jump to non-ground eigenstate under strong gradient (H-mode). The unconventional mode structure can significantly reduce the effective correlation length and thus the turbulent transport. This viewpoint can provide a mechanism to understand the previous nonlinear simulations in this paper. We note the critical gradient for the frequency jump is $R_0/L_T \simeq 70$, which is around the experimental L-H transition gradient $R_0/L_T \simeq 40 - 120$ [24, 28]. The low and high frequencies from the simulation also quantitatively agree with the characteristic frequencies of the electrostatic turbulence for typical HL-2A L-mode and H-mode, i.e., $\sim 20\text{kHz}$ and $\sim 80\text{kHz}$, respectively [23].

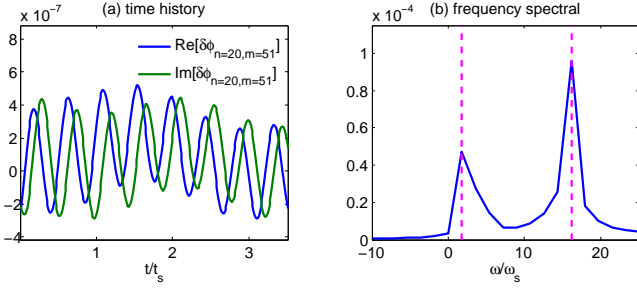


FIG. 5: The time history (a) and frequency spectral (b) for the Fourier component ($n = 20$, $m = 51$) of electrostatic potential in the linear simulation with $R_0/L_T = 75$.

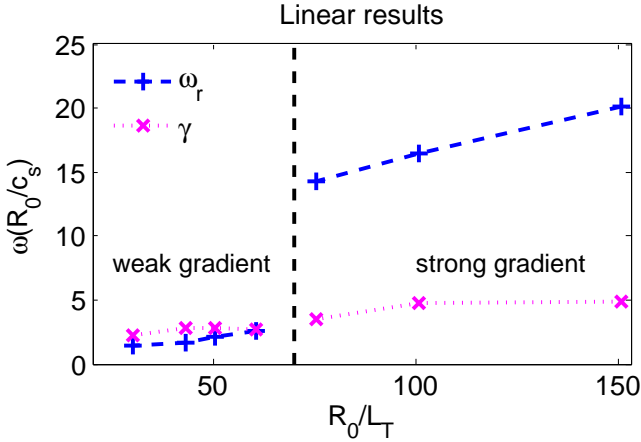


FIG. 6: Linear real frequency and growth rate for most unstable mode under different temperature gradients using typical HL-2A parameters with selected toroidal mode number $n = 20$.

The detailed linear results, especially the unconventional mode structures and eigenstate jump, have been reported in Refs. [23, 27], where the mirco-instability is identified as trapped electron modes (TEMs) [29, 30]. It has also been recently reported that the turbulence (usually also TEM) jump from low frequency to high frequency during the L-H transition for experiments such as DIII-D [31] or EAST [32]. Other simulations also discussed the possible important roles of resistive ballooning mode [33] or the large diamagnetic frequency [34], but they did not show a clear sudden change of transport characteristics as the present work does.

So far we have discovered the coexistence of both linear and nonlinear critical gradients. However, the linear critical gradient ($R_0/L_T = 75$) is larger than the nonlinear critical gradient ($R_0/L_T = 25$). There could have two reasons for this difference. The first one is shown by Fig. 6: the linear growth rate ceases to grow before the linear discontinuity occurs. The second reason is associated with the following inverse poloidal spectral cascade in the nonlinear saturation of turbulence. We carry out a nonlinear gyrokinetic simulation under strong gra-

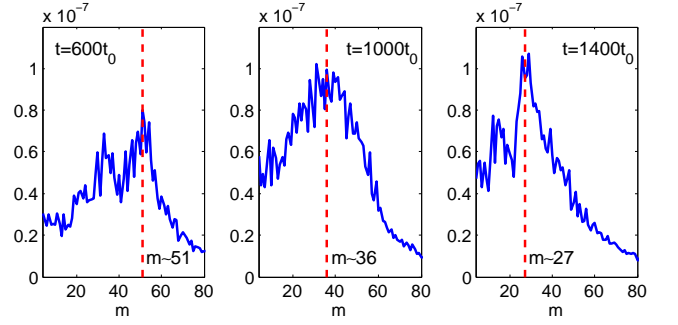


FIG. 7: The poloidal spectral cascade from high to low mode number during nonlinear saturation.

dient with a typical HL-2A H-mode experimental value $R/L_T = 150$. As shown in Fig. 7, the peaking m downshifts from a larger number to a smaller number during the nonlinear saturation process, which demonstrates a nonlinear inverse cascade in the poloidal spectrum. The peaking m at a later saturation stage ($t = 1400t_0$, steady state, where t_0 is time step size) is $m = 10 - 40$, whose value is close to the experimental value $m = 14 - 33$ [23, 24].

In conclusion, via first principle gyrokinetic simulation we have found a trend reversal in the transport coefficients and a discontinuous change of the slope of the transport flux in the strong-gradient regime of magnetic fusion plasmas, indicating that a small increase of the heat flux can lead to a large increase of the gradient, similar to a second order phase transition [5]. We also found that there exist both linear and nonlinear critical gradients for the discontinuity of the transport characteristics. In the linear simulation, with increase of the edge gradient, the most unstable mode jumps from the ground eigenstate to another eigenstate. The unconventional mode structure associated with the latter can effectively reduce the correlation length and thus the transport coefficients. This result is confirmed by the nonlinear simulation, which shows that the radial correlation length is indeed reduced in the strong gradient regime, and a turning point (the nonlinear critical gradient) indeed appears in the transport coefficients. The reduction of the critical gradients and transport coefficient can be crucial to the formation of the H-mode external transport barrier (ETB) as well as the L-H transition. This result therefore suggests a new pathway to the H-mode regime, namely without the need of shear and/or zonal flows. In fact, experiments have also raised doubt on the need of the latter for the L-H transition [25, 35], and the corresponding fluid models for the L-H transition are also not fully convincing [34]. Finally, we note that gyrokinetic simulations can provide quantitative outputs for closer comparison with experimental results. In fact, the critical gradient, characteristic frequency and poloidal mode number from our nonlinear simulation are consistent with

the HL-2A experiments. Moreover, for further resolving the mystery of the L-H transition, other effects such as flow shear, electromagnetic perturbations, self-consistent evolution of the plasma profiles, etc. can also be included in the gyrokinetic simulation.

Acknowledgments HSX would like to thank D. F. Kong, G. S. Xu, and K. K. Barada for providing the experimental information from the HL-2A, EAST, and DIII-D tokamaks. We would like to thank L. Chen, G. Y. Fu and M. Y. Yu of ZJU, P. H. Diamond of UCSD and X. Q. Xu of LLNL for useful discussions. This work is supported by the National Magnetic Confinement Fusion Energy Research Program under Grant Nos. 2015GB110000, 2013GB111000, the China NSFC under Grant Nos. 11575158, the Recruitment Program of Global Youth Experts, and the US DOE SciDac GSEP Center.

* Email: huashengxie@gmail.com

† Email (Corresponding author): yxiao@zju.edu.cn

- [1] F. Wagner et al., Phys. Rev. Lett. **49**, 1408 (1982).
- [2] C. R. Or and F. H. Busse, J. Fluid Mech. **174**, 313 (1987); M. E. McIntyre, J. Atmos. Terr. Phys. **51**, 29 (1989).
- [3] K. Ikeda, Nucl. Fusion **47** (2007).
- [4] F. Wagner, Plasma Phys. Control. Fusion, **49**, B1 (2007).
- [5] Translated and reprinted from Landau L.D. Collected Papers (Nauka, Moscow, 1969), Vol. 1, pp. 234C252. Originally published in Zh. Eksp. Teor. Fiz. **7**, pp. 19C32 (1937)
- [6] H. Biglari, P. H. Diamond and P. W. Terry, Phys. Fluids B **2**, 1 (1990).
- [7] T. S. Hahm, Phys. Plasmas, **1**, 2940 (1994).
- [8] R. E. Waltz, G. D. Kerbel and J. Milovich, Phys. Plasmas, **1**, 2229 (1994).
- [9] J. Li and Y. Kishimoto, Phys. Rev. Lett., **89**, 115002 (2002).
- [10] S. I. Itoh, K. Itoh and A. Fukuyama, Nuclear Fusion, **33**, 1445 (1993).
- [11] E. J. Kim and P. H. Diamond, Phys. Rev. Lett., **90**, 185006 (2003).
- [12] Rogers et al., Phys. Rev. Lett., **81**, 4396 (1998). Xu et al. Phys. Plasmas **7**, 1951 (2000). Park et al. Phys. Plasmas **22**, 032505 (2015). L. Chone et al, Nuclear Fusion, **55**, 073010 (2015). Li et al. Phys. Plasmas **22**, 112305 (2015).
- [13] A. J. Brizard and T. S. Hahm, Rev. Mod. Phys., **79**, 421 (2007).
- [14] W. W. Lee, Journal of Computational Physics, **72**, 243 (1987).
- [15] Z. Lin and T. S. Hahm, Phys. Plasmas, **11**, 1099 (2004).
- [16] Z. Lin et al., Science, **281**, 1835 (1998).
- [17] W. Horton, Rev. Mod. Phys., **71**, 735 (1999).
- [18] A. M. Dimits et al, Phys. Plasmas, **7**, 969 (2000).
- [19] B. Scott, Plasma Phys. Control. Fusion, **48**, B277 (2006).
- [20] G. Rewoldt, Z. Lin and Y. Idomura, Computer Physics Communications, **177**, 775 (2007).
- [21] Y. Xiao and Z. Lin, Phys. Rev. Lett., **103**, 085004 (2009).
- [22] I. Holod and Z. Lin, Phys. Plasmas, **20**, 032309 (2013).
- [23] H. S. Xie, ‘Numerical Simulations of Micro-turbulence in Tokamak Edge’, PhD thesis, Zhejiang University, 2015. <http://hsxie.me/files/thesis>
- [24] D. F. Kong et al., Nucl. Fusion, **57**, 014005 (2017).
- [25] T. Kobayashi, et al., Phys. Rev. Lett., **111**, 035002 (2013).
- [26] W. Horton, *Turbulent Transport in Magnetized Plasmas World*, Scientific Publishing Company, 2012.
- [27] H. S. Xie and Y. Xiao, Phys. Plasmas, **22**, 090703 (2015).
- [28] F. Ryter et al., Plasma Phys. Control. Fusion, **58**, 014007 (2016); R. A. Moyer et al., Phys. Plasmas, **2**, 2397 (1995).
- [29] B. Coppi and G. Rewoldt, Phys. Rev. Lett., **33**, 1329 (1974).
- [30] P. J. Catto and K. T. Tsang, Phys. Fluids, **21**, 1381 (1978).
- [31] K. K. Barada, private communication, APS-DPP, Savannah, 2015.
- [32] G. S. Xu et al, Phys. Plasmas, **19**, 122502 (2012); H. Q. Wang et al, Nucl. Fusion, **52**, 123011 (2012).
- [33] C. Bourdelle et al, Nucl. Fusion, **55**, 073015 (2015).
- [34] B. Scott, A. Kendl and T. Ribeiro, Contrib. Plasma Phys., **50**, 228 (2010).
- [35] S. J. Zweben, et al, Phys. Plasmas, **17**, 102502 (2010).